Effect of Evaporation Time on the Pervaporation Characteristics Through Homogeneous Aromatic Polyamide Membranes. I. Pure Water Permeation and Membrane Characterization by Sorption Measurements*

AKIHIRO YAMASAKI, R. K. TYAGI, A. FOUDA,† and T. MATSUURA‡

Institute for Environmental Research and Technology, National Research Council of Canada, Ottawa, Ontario K1A 0R6 Canada

SYNOPSIS

The pervaporation of pure water through homogeneous aromatic polyamide membranes was investigated. The structure of the prepared membranes was controlled by varying the solvent evaporation times before the gelation step from 5 min to 240 min. The permeation flux of pure water decreased rapidly when the solvent evaporation time increased from 5 min to 30 min, and the decrease was rather moderate at higher evaporation times. Vapor and liquid sorption measurements were used to characterize the membranes. The amount of vapor sorption at a given relative pressure increased with an increase in the solvent evaporation time. The specific surface area of the membranes, calculated from the vapor sorption isotherm, increased with evaporation time up to 30 min, and remained constant thereafter. Liquid sorption volume, on the other hand, decreased monotonically with an increase in evaporation time. The formation of channels in the membrane is used to explain the morphology change during the solvent evaporation. The increase in the solvent evaporation time gradually increases the number of the channels in the membrane and decreases their average size. Good correlation was observed between the average size of the channels (represented by the ratio of specific volume to the specific surface area) and the parameters associated with pervaporation transport. © 1995 John Wiley & Sons, Inc.

INTRODUCTION

Pervaporation has been recognized nowadays as one of the most versatile membrane separation processes.[1] In particular, pervaporation is used for the dehydration of organic solvents and the removal of a small quantity of organic compounds from water. A potentially useful application of pervaporation is separation of azeotropic mixtures.

Because the fabrication of the membrane is the key to the success of this process, a number of new polymeric materials have been synthesized and tested for pervaporation performance. Interestingly, however, the study of the effects of variables involved in the membrane preparation procedure was almost completely neglected. This is in contrast to reverse osmosis, ultrafiltration, and gas separation membranes.[2-9] One of the reasons may be that commercially available pervaporation membranes are composite membranes like GFT membrane,[10] where a thin dense film is coated on a porous substrate membrane. The thin dense layer is considered to be homogeneous, and the intrinsic permeation property of the polymer that constitutes the dense layer is thought to govern the selectivity of the composite membrane. Then, the method to prepare the thin dense layer is not considered to affect the membrane performance.

* NRCC No. 37592

† To whom correspondence should be addressed.

‡ Industrial Membrane Research Institute, the University of Ottawa, Ottawa, Ontario, K1N 6N5 Canada.

Journal of Applied Polymer Science, Vol. 57, 1473–1481 (1995)
© 1995 John Wiley & Sons, Inc. CCC 0021-8995/95/121473-09

The thin dense layer looks, indeed, homogeneous and structureless when observed under an electron microscope. However, the above observation does not necessarily preclude the possibility of the presence of the polymeric structure in a scale smaller than the resolution of scanning electron microscopy (SEM), and different structures may exist, depending on the variables involved in the preparation procedure of the homogeneous membranes. Examples of such variables are solvent used to make polymer solutions, polymer concentration in the solution, nature and amount of the additive in the polymer solution, solvent evaporation time, evaporation temperature, and amount of the residual solvent.

The objective of this work is to investigate the effect of the evaporation time on the structure of pervaporation membranes and on their pervaporation performance. The pervaporation performance of pure water was strongly affected by the evaporation time of the solvent, and a trend was observed between the pervaporation permeability and the evaporation time. These results suggest the changes of the membrane structure due to the difference in the solvent evaporation time. Because all the membranes studied look homogeneous, SEM technique can no longer serve as a tool to observe the difference in the membrane structure. Instead, adsorption data of water both in liquid and vapor phase were used to investigate the membrane structure. The pervaporation data of water were further correlated to the parameters that represent the membrane structure.

EXPERIMENT

Materials and Membrane Preparation

The polymer used in this study was poly-*m*-phenylene-iso(70)-*co*-tere(30)-phtalamide, which was synthesized in our laboratory according to the method reported elsewhere.[11] Membranes were prepared as follows: casting the solution on a glass plate, evaporation of the solvent, and gelation in cold water. The casting solution consists of 10.3 wt % polymer, 3.8 wt % LiCl, and 85.9 wt % dimethylacetamide (DMAc). LiCl was used to enhance the dissolution of polymer in the solvent. Casting thickness was 2 mils (50.4 μm). The evaporation of the solvent was carried out at 95°C in an air atmosphere. The evaporation time was changed from 5 min to 240 min. After gelation, membranes were kept in pure water for several days to leach out LiCl. It was confirmed from atomic analysis that LiCl in the membrane was perfectly taken away into water in several days. The membranes were homogeneous and no visible pores were observed under SEM. The thickness of dry membranes was measured through the SEM image, and it was in the range of 5 ± 0.5 μm for all membranes studied.

Pervaporation

A schematic diagram for the pervaporation experiment apparatus is shown in Figure 1. The membrane (effective permeation area is 9.4×10^{-4} m^2) was placed in the stainless steel cell of which the temperature was kept 25°C by a constant temperature bath. The vacuum of the downstream side was controlled by a needle valve. The permeate was collected in a trap cooled by liquid nitrogen. The permeation rate was calculated by the weight measurement. Each run was carried out for at least 4 h after the attainment of the steady-state permeation.

Liquid Sorption

The water-wet membrane was dried in a vacuum oven for 24 h at 60°C before weighing. Then, the membrane was placed in a vacuum oven again, dried for another 24 h, and weighed. There was no change between these two weight measurements. For the liquid sorption experiments, the membrane was immersed in pure water, the temperature of which was maintained at 25°C in a constant temperature bath. After 24 and 48 h of immersion, the membrane was taken out of water, blotted quickly, and weighed. There was no weight change between 24 and 48 h. It was, therefore, confirmed that sorption equilibrium had been established within 24 h.

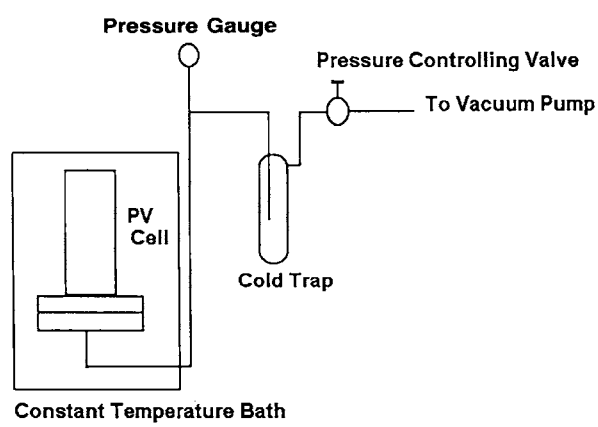

Figure 1 Schematic diagram for the pervaporation experimental apparatus.

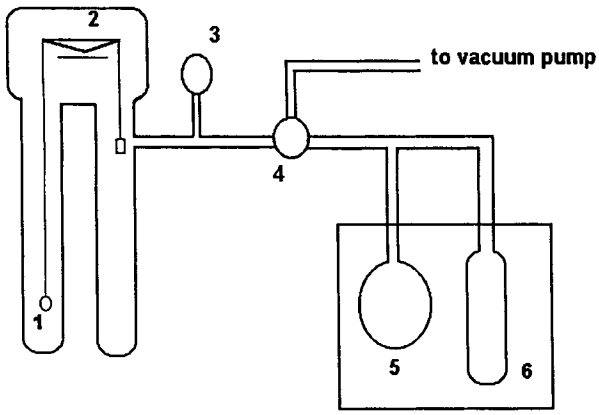

Figure 2 Schematic diagram for the vapor sorption measurement apparatus.

Vapor Sorption

Vapor sorption equilibrium was established by using an apparatus that included Cahn micro balance (Fig. 2). A membrane of known dry weight (typically 100 mg) was loaded. After evacuation of the chamber, water vapor was introduced to the latter chamber from the vapor feeding unit that consisted of a liquid chamber and a vapor chamber. The attainment of sorption equilibrium was confirmed by monitoring the weight change of the membrane. In all cases, no further weight changes were observed after 2 h. The temperature of the system was kept at 25°C by a water circulated jacket.

RESULTS AND DISCUSSION

Pervaporation

In Figure 3, water flux was plotted against the downstream pressure for membranes prepared with a different evaporation time. Although the flux decreased with an increase in the evaporation time, the shape of each curve was exactly the same; i.e., it consists of a parabolic part at the downstream pressure below 3 kPa and a linear part at the downstream pressure above 3 kPa. It should be noted that the vapor pressure of water at 25°C is approximately 3 kPa.

It is known that the above functional form can be represented by the equations,[12]

$$J = (A/l)\,(p_2 - p*) + (B/l)(p*^2 - p_3^2), \quad \text{when } p_3 < p* \qquad (1)$$

$$J = (A/l)(p_2 - p_3), \quad \text{when } p_3 \geqslant p* \qquad (2)$$

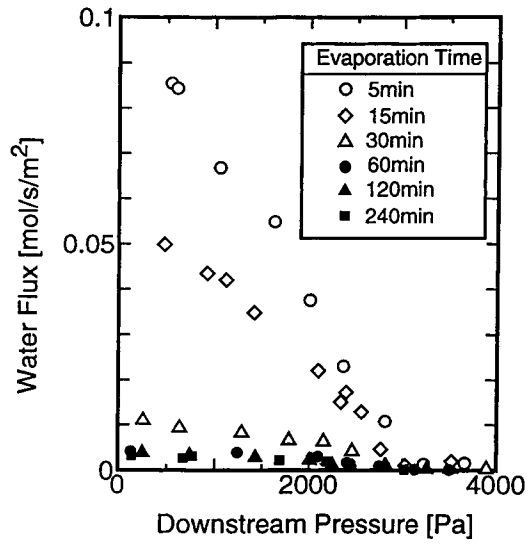

Figure 3 Effect of evaporation time on water flux.

where J, p_2, $p*$, and p_3 are the water flux [mol/m^2/s], upstream pressure [Pa], saturation vapor pressure of water [Pa], and downstream pressure [Pa], respectively. A/l and B/l are the parameters concerning liquid transport [mol/m^2/s/Pa] and vapor transport [mol/m^2/s/Pa^2], respectively. The numerical values of A/l and B/l were, therefore, obtained by the fitting of experimental data, and the results are summarized in Table I. Both parameters decreased rapidly until the evaporation time reached 30 min. Above 30 min, the change was more moderate.

The above fitting enables the normalization of the permeation flux. Each curve was extrapolated to $p_3 = 0$, and J corresponding to $p_3 = 0$ was set equal to J_0. According to Eq. (1),

$$J_0 = (A/l)(p_2 - p*) + (B/l)p*^2 \qquad (3)$$

Then, the normalized flux, J/J_0, in the range of $p_3 < p*$ was plotted vs. relative pressure x_3

Table I Pervaporation Transport Parameters

Evaporation Time (min)	A/l (mol/s/m^2/Pa)	B/l (mol/s/m^2/Pa^2)
5	17.6×10^{-9}	57.8×10^{-10}
15	8.04	30.6
30	4.91	9.28
60	3.32	4.63
120	2.30	3.79
240	1.07	2.78

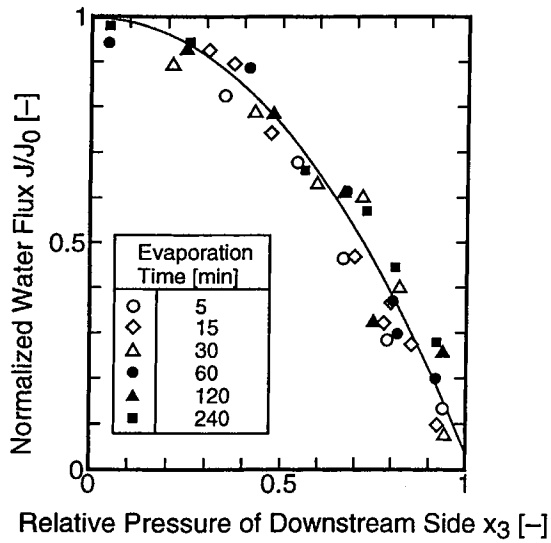

Figure 4 Normalized water flux vs. relative pressure.

($= p_3/p*$) of the downstream side in Figure 4. Figure 4 shows that the normalized flux below the saturation pressure ($x_3 < 1$) can be represented by a single correlation line, regardless of the evaporation time.

Sorption Experiments

Figure 5 shows the vapor sorption isotherms for the membranes with 5, 30, and 240 min evaporation times. The amount of water vapor adsorbed at a given relative vapor pressure ($p/p*$) increased with an increase in the evaporation time.

In Figure 6, data from Figure 5 were replotted according to the BET equation,[13]

$$p/q(p* - p) = (1/q_m c) + \{(1 - c)/q_m c\}\ (p/p*) \quad (4)$$

where p, $p*$, q, and q_m are vapor pressure of water [Pa], saturation vapor pressure of water [Pa], amount of water adsorbed to unit weight of the membrane sample [mol/kg], and monolayer capacity [mol/kg], respectively. The quantity c can be expressed as,[13]

$$c = \exp\{(E_1 - E_L)/RT\} \quad (5)$$

where E_1 is the heat of sorption of the first adsorption layer [J/mol], and E_L is the heat of evaporation of water [J/mol], R is the gas constant [J/mol/K], and T is the absolute temperature [K]. The straight line relationship obtained in Figure 6 indicates that Eq. (4) is valid in a range of the relative pressure, $p/p*$, lower than 0.35. The parameters q_m and c were

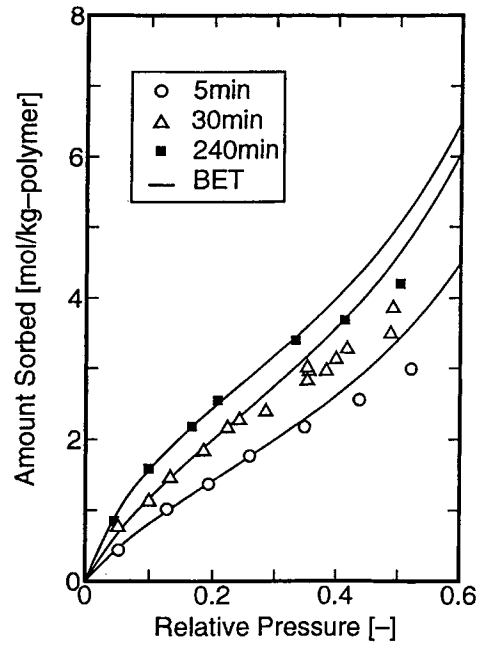

Figure 5 Water vapor sorption isotherm.

obtained from the intercept and the slope of the BET plot.

The parameters q_m and c obtained were plotted vs. evaporation time in Figure 7. Note that Figure 7 includes data for evaporation times other than 5, 30, and 240 min. Whereas q_m increased until evaporation time reached 30 min and leveled off there-

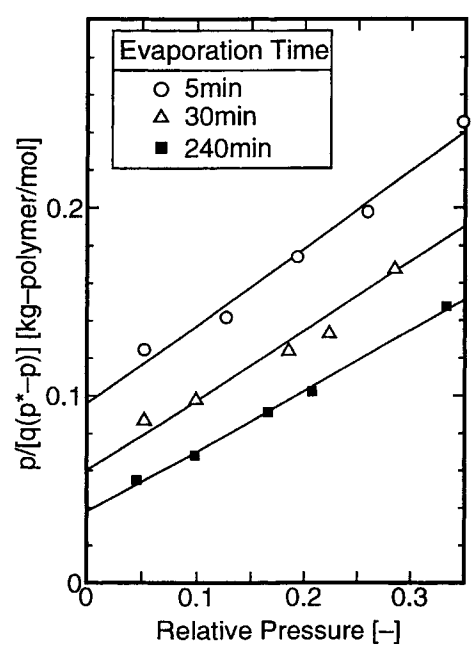

Figure 6 BET plot for water sorption.

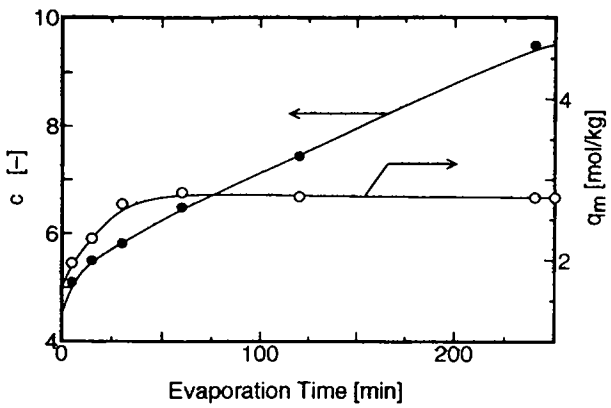

Figure 7 Effect of evaporation time on the BET parameters.

after, c kept increasing with an increase in evaporation time. The constant monolayer capacity, q_m, after 30 min evaporation time means that the area utilized for the adsorption of water vapor was also constant for the evaporation time greater than 30 min.

Equation (4) was further rearranged to,

$$q = cq_m(p/p*)/[\{1 - (p/p*)\} \times \{1 - (p/p*) + c(p/p*)\}] \quad (6)$$

and q was calculated as a function of $(p/p*)$ using the parameters q_m and c obtained above. The results are given in Figure 5 for evaporation times 5, 30, and 240 min as solid lines. Note that q_m and c were obtained from the BET plot corresponding to $p/p* < 0.35$. The calculated isotherms showed positive deviations at $p/p*$ values higher than 0.35, because an infinite number of adsorption layers was allowed in the derivation of Eq. (4). In reality, only a limited space should be available for adsorption in the polymer, which restricts the number of adsorption layers. The upward deviation became greater as the evaporation time increased, which means that the volume of the space available for the multilayer adsorption became less as the evaporation time increased.

The continuous decrease in the adsorption volume is supported by Figure 8, where the effect of the evaporation time on the liquid water sorption is illustrated. The amount of liquid water sorption kept decreasing even when the evaporation time was more than 30 min, although the decrease became more moderate after 60 min. This is in contrast to the conclusion from Figure 7 that the specific surface area for vapor adsorption increased with an increase in the evaporation time up to 30 min and did not change after 30 min of evaporation time. These results can be explained based on the morphology change of the membrane represented by the change in the number and the size (radius) of cylindrical channels in homogeneous membranes. Obviously, the mass transport takes place through such channels in pervaporation, whatever the origin of them are. The specific surface area for vapor sorption (calculated from monolayer capacity, q_m) can be related to the surface area of the channels, and the liquid sorption amount can be related to the volume of the channels. Set symbols n [1/kg], r[m], and L[m] for the number in a unit weight membrane, radius, and the length of the cylindrical channel, respectively. Let us also use S[m^2/kg] and V[m^3/kg] for the specific area and the specific volume of the membrane, respectively. Let subscript 30 and t (> 0) denote 30 min and evaporation time, respectively. Then, the specific surface area at evaporation time 30 min and t min can be expressed as,

$$S_{30} = 2\pi n_{30} r_{30} L \quad (7)$$

$$S_t = 2\pi n_t r_t L \quad (8)$$

The specific volume can be expressed as,

$$V_{30} = \pi n_{30} r_{30}^2 L \quad (9)$$

$$V_t = \pi n_t r_t^2 L \quad (10)$$

The length of the channel, L can be assumed to be constant, regardless of the evaporation time, because the membrane thickness was in the range of 5 ± 0.5 μm. When $t < 30$, from the results in Figures 7 and 8,

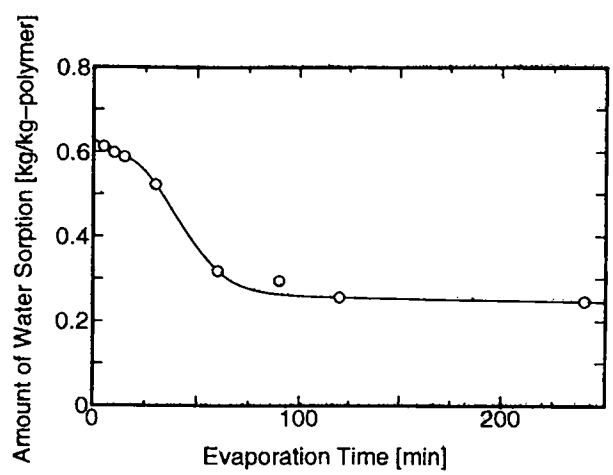

Figure 8 Effect of evaporation time on water (liquid) sorption.

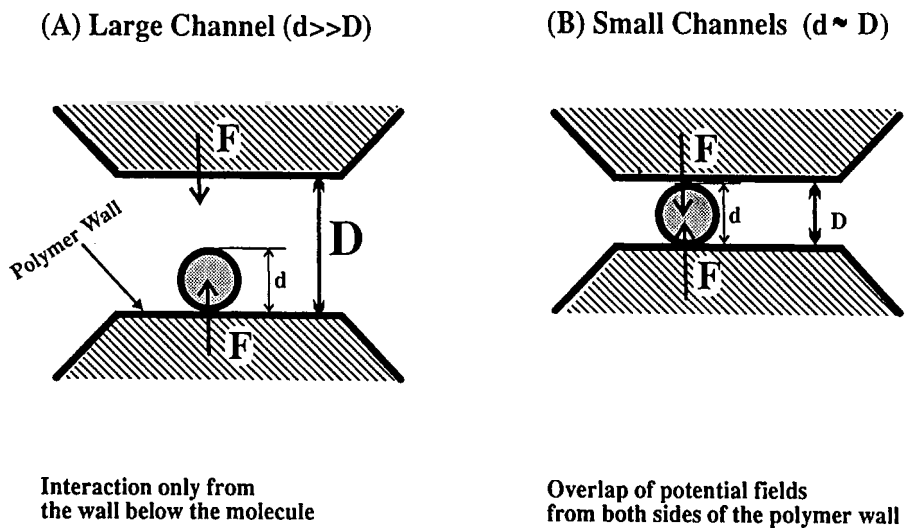

Figure 9 Effect of channel size on the interaction of adsorbed water molecules and the channel wall.

$$S_{30} > S_t \tag{11}$$

$$V_{30} < V_t \tag{12}$$

Substitution of Eqs. (7) and (8) into Eq. (11) yields,

$$n_{30}r_{30} > n_t r_t \tag{13}$$

Substitution of Eqs. (9) and (10) into (12) yields,

$$n_{30}r_{30}^2 < n_t r_t^2 \tag{14}$$

Division of Eq. (14) by Eq. (13) yields,

$$r_{30} < r_t \tag{15}$$

Also from Eqs. (13) and (15), we obtain,

$$n_{30} > n_t \tag{16}$$

Therefore, the increase in the surface area (monolayer capacity) and the decrease in the liquid sorption amount below 30 min can be explained in terms of the decrease in the size and the increase in the number of the channels.

When $t > 30$, the following can be drawn from the sorption experiments,

$$S_{30} = S_t \tag{17}$$

$$V_{30} > V_t \tag{18}$$

Division of Eq. (18) by Eq. (17) yields,

$$V_{30}/S_{30} > V_t/S_t \tag{19}$$

Then, using Eqs. (7), (8), (9), (10), and (19), we obtain,

$$r_{30} > r_t \tag{20}$$

and from Eqs. (7), (8), (17), and (20),

$$n_{30} < n_t \tag{21}$$

The morphology change above 30 min should also be represented by a decrease in the average size of the cavity and an increase in the number of the channels.

The decrease in the size of the channels can be also supported by the results shown in Figure 7, where c increases with an increase in the evaporation time. According to Eq. (5), the increase in c indicates the increase in the heat of sorption of the first layer, E_1. As shown in Figure 9 schematically, the molecules in the first adsorbed layer in a smaller channel feel the interaction forces not only from the lower parts of the channel wall but also from the upper parts. Thus, the interaction force should increase as the channel size decreases, resulting in an increase in the heat of adsorption.

Let us now discuss the mechanism of the morphology change of the membrane. Figure 10 shows the change of the weight of the cast film with solvent evaporation time. The figure indicates that solvent evaporation takes place rapidly up to 30 min of

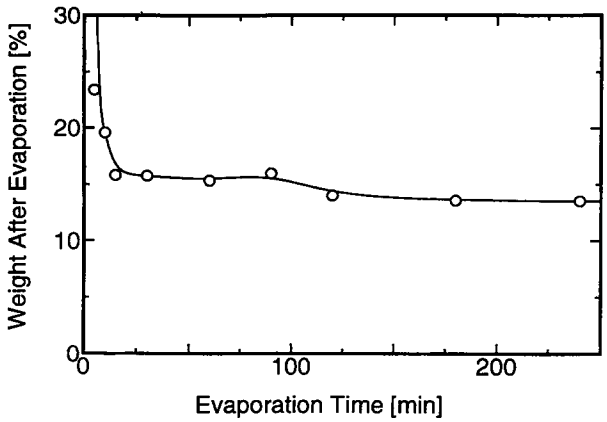

Figure 10 Weight change of the casting solution.

evaporation time, and the evaporation becomes slow thereafter. These two distinct evaporation stage should corresponds to the different manners of the membrane morphology change.

In the process of membrane formation, we start from a mixture in which the mol fraction of polymer is so low that polymer and solvent are completely miscible. As the solvent evaporates, the polymer mol fraction increases and the composition of the binary system moves into the immiscible region and the phase separation starts to occur. Because we have started from a dilute polymer solution, it is likely that the polymer-rich phase is dispersed in a continuous polymer-poor phase and, thus, forms droplets of the polymer-rich phase [Fig. 11(A)]. At the earlier stage of solvent evaporation, fast evaporation from the polymer-poor phase should be dominant because the solvent–polymer interaction is stronger than solvent–solvent interaction. Evaporation from the polymer-poor phase results in the formation of a small number of large cavities (or channels), which are surrounded by the droplets of polymer-rich phase [Fig. 11(B)]. With an increase in the evaporation time, the distance between the droplets become smaller and large cavities split into smaller cavities. This process results in the decrease in the channel size and the increase in the number of channels. The above morphology change should correspond to the one below 30 min of evaporation time. At the same time, the solvent evaporation takes place from the droplets, rendering its size smaller. However, the evaporation rate is much smaller because of the stronger interaction between the polymer and the solvent.

The droplets are considered to be a spherical network of polymer segments swollen by solvent and hereafter called polymer aggregates. As the solvent evaporation further proceeds, the solvent continues to leave the droplet of the polymer-rich phase reducing the droplet size, until the droplet become completely solvent free. As the aggregate size decreases, the vacant void space can no longer be maintained, and restructuring of the aggregates should take place, which results in the disappearance of large void spaces and in the formation of many smaller internodular void spaces [Fig. 11(C)]. This process should correspond to the slower evaporation process below 30 min of evaporation time, which

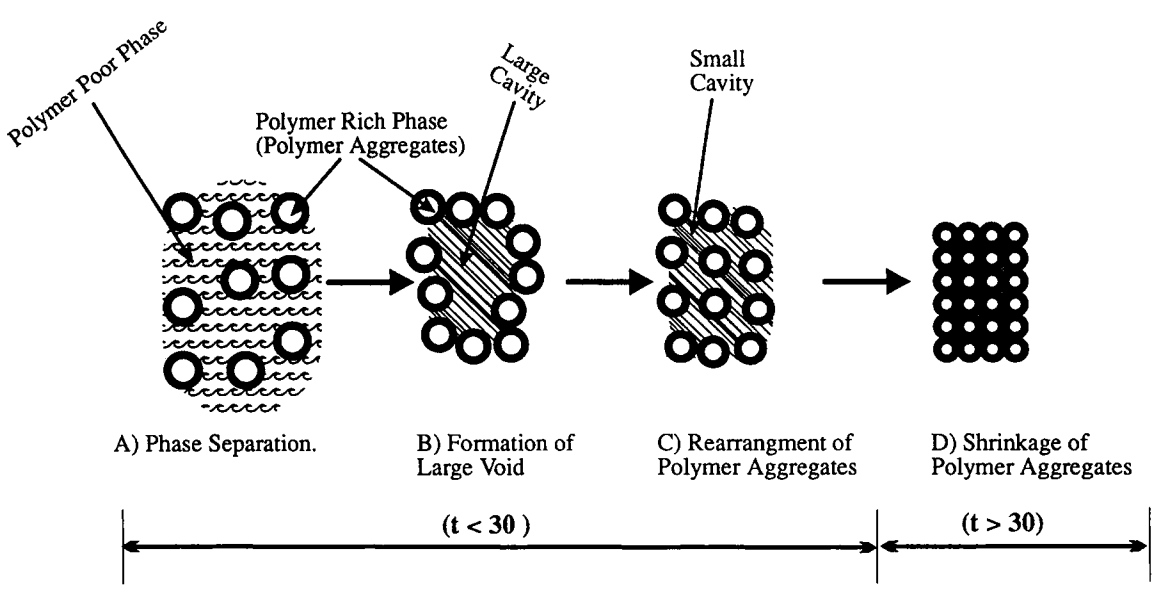

Figure 11 Effect of evaporation time on the membrane structure.

also resulted in the decrease in the channel size and the increase in the number of the channels. When the evaporation procedure is completed, the membrane structure, therefore, consists of closely packed polymer aggregates with internodular void spaces [Fig. 11(D)].

Correlation between Pervaporation Performance and Membrane Morphology

Equations (8) and (10) imply that the quantity V_t/S_t is a measure of the size of the channel where the transport takes place. An attempt was, therefore, made to calculate V_t/S_t from sorption data and to correlate the latter quantity to the transport parameters obtained from pervaporation experiments. V_t can be calculated from the liquid water sorption data, assuming that the density of water in the polymer is the same as that of water in the bulk phase. S_t was calculated from the data on $q_m(t)$ that was obtained from the vapor sorption experiment as follows. Setting the surface area occupied by a single water molecule equal to a [m^2/molecule], S_t[m^2/kg] becomes,

$$S_t = aq_m(t)N \tag{22}$$

where N is Avogadro number [molecule/mol]. The quantity a can be calculated by Eq. (23),[13]

$$a = 1.091 \times (M/\rho N)^{2/3} \tag{23}$$

where M is molecular weight [kg/mol], ρ [kg/m^3] is the liquid density. For water molecule, a is equal to 10.5×10^{-20} [m^2/molecule].

V_s/S_t so calculated was plotted vs. transport parameters A/l and B/l in Figure 12. Both transport parameters increase linearly with an increase in V_t/S_t. The values for V_t/S_t in Figure 12 are equal to or greater than 30×10^{-10} m and seem to be too large for pervaporation membranes. It should be noted that an assumption was made in the above calculation that the morphology of the polymer under the condition of the BET adsorption experiments, where $p/p* < 0.35$, and under the condition of liquid water sorption is exactly equal. Obviously, this assumption is too crude. The polymer swells more in liquid water and the value for V_t was greatly overestimated as compared with the volume available for vapor sorption. Hence, V_t/S_t is also an overestimation of the radius of the channel.

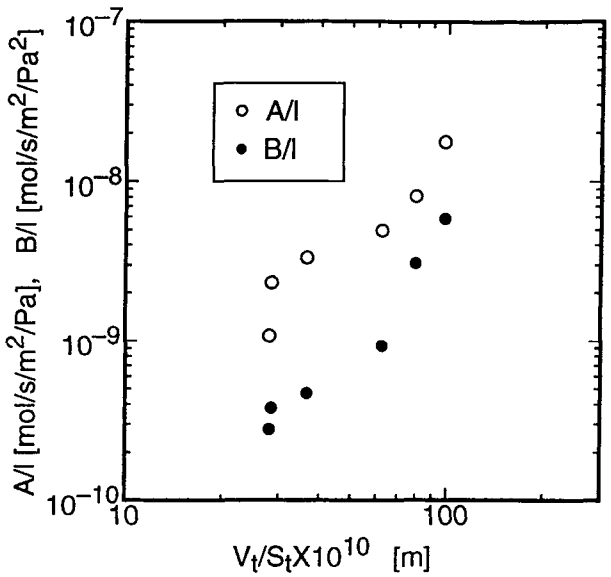

Figure 12 Relationship between V/S and A/l, B/l.

CONCLUSIONS

From the results of sorption and pervaporation experiments described above, the following conclusions can be drawn.

(1) The morphology of the homogeneous polyamide membrane, when characterized by the size and the number of cylindrical channels, changes as the solvent evaporation progresses in the following way. (a) The size of the channels decreases; (b) the number of the channels increases. (2) There is a correlation between the parameters associated with the pervaporation transport of pure water and the channel diameter.

The above conclusions are restricted to the dense symmetric aromatic polyamide membranes prepared by solvent evaporation.

REFERENCES

1. R. Y. M. Huang (Ed.), *Pervaporation Membrane Separation Processes,* Elsevier, Amsterdam, 1991.
2. K. Chan, T. Matsuura, and S. Sourirajan, *Ind. Eng. Chem. Prod. Res. Dev.,* **21,** 605 (1982).
3. K. Chan, T. Liu, T. Matsuura, and S. Sourirajan, *Ind. Eng. Chem. Prod. Res. Dev.,* **23,** 492 (1984).
4. T. Matsuura and S. Sourirajan, in *Reverse Osmosis and Ultrafiltration,* ACS Symposium Series, No. 281, American Chemical Society, Washington, DC, 1985, p. 1.
5. T. D. Nguyen, K. Chan, T. Matsuura, and S. Sourirajan, *Ind. Eng. Chem. Pros. Res. Dev.,* **24,** 655 (1985).

6. T. D. Nguyen, T. Matsuura, and S. Sourirajan, *Chem. Eng. Commun.*, **54,** 17 (1987).
7. T. D. Nguyen, T. Matsuura, and S. Sourirajan, *Chem. Eng. Commun.*, **57,** 351 (1987).
8. T. D. Nguyen, T. Matsuura, and S. Sourirajan, *Chem. Eng. Commun.*, **88,** 91 (1990).
9. Z. Zhenxin and T. Matsuura, *J. Colloid Interface Sci.*, **147,** 307 (1991).
10. W. Gudernatsch, Th. Menzel, and H. Strathmann, *J. Membr. Sci.*, **61,** 19 (1991).
11. Blais, P. in *Reverse Osmosis Synthetic Membranes,* S. Sourirajan, Ed, National Research Council of Canada, Ottawa, 1977, p. 167.
12. T. Okada and T. Matsuura, *J. Membr. Sci.*, **59,** 133 (1991).
13. S. J. Gregg and K. S. W. Sing, *Adsorption, Surface Area, and Porosity,* Academic Press, London, 1967.

Received December 16, 1994
Accepted April 21, 1995